

1 **REVISION 1**

2
3 **Vanadio-oxy-dravite, $\text{NaV}_3(\text{Al}_4\text{Mg}_2)(\text{Si}_6\text{O}_{18})(\text{BO}_3)_3(\text{OH})_3\text{O}$, a new mineral**
4 **species of the tourmaline supergroup**

5
6 FERDINANDO BOSI¹, HENRIK SKOGBY², LEONID REZNITSKII³, AND ULF HÅLENIUS²

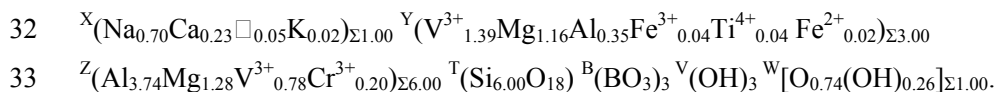
7
8 ¹Dipartimento di Scienze della Terra, Sapienza Università di Roma, P.le A. Moro, 5, I-00185 Rome,
9 Italy

10 ²Department of Geosciences, Swedish Museum of Natural History, Box 50007, SE-10405 Stockholm,
11 Sweden

12 ³Russian Academy of Science. Siberian Branch, Institute of the Earth's crust, Lermontova str., 128,
13 Irkutsk, Russia

14
15
16
17
18 **ABSTRACT**

19 Vanadio-oxy-dravite, $\text{NaV}_3(\text{Al}_4\text{Mg}_2)(\text{Si}_6\text{O}_{18})(\text{BO}_3)_3(\text{OH})_3\text{O}$, is a new mineral of the
20 tourmaline supergroup. It is found in metaquartzites of the Pereval marble quarry (Sludyanka,
21 Lake Baikal, Russia) in association with quartz, Cr-V-bearing tremolite and mica, diopside –
22 kosmochlor – natalyite, Cr-bearing goldmanite, escolaitite – karelianite, dravite – oxy-
23 vanadium-dravite, V-bearing titanite and rutile, ilmenite, oxyvanite – berdesinskiite,
24 shreyerite, plagioclase, scapolite, zircon, pyrite and an unnamed oxide of V, Cr, Ti, U and Nb.
25 Crystals are green, transparent with a vitreous luster, pale green streak and conchoidal
26 fracture. Vanadio-oxy-dravite has a Mohs hardness of approximately 7½, and a calculated
27 density of 3.14 g/cm³. In plane polarized light, vanadio-oxy-dravite is pleochroic (O = yellow
28 green and E = pale olive green) and uniaxial negative: $\omega = 1.693(5)$, $\epsilon = 1.673(5)$ Vanadio-
29 oxy-dravite is rhombohedral, space group $R3m$, with the unit-cell parameters $a = 16.0273(3)$, c
30 $= 7.2833(1)$ Å, $V = 1620.24(5)$ Å³, $Z = 3$. Crystal-chemical analysis resulted in the empirical
31 structural formula:



34 The crystal structure of vanadio-oxy-dravite was refined to an *R*1 index of 1.70% using
35 1800 unique reflections collected with *MoK α* X-radiation. Ideally, vanadio-oxy-dravite is
36 related to oxy-dravite and oxy-vanadium-dravite by the homovalent substitution $\text{V}^{3+} \leftrightarrow \text{Al}^{3+}$.
37 Tourmaline with chemical compositions classified as vanadio-oxy-dravite can be either Al-
38 dominant or V-dominant as a result of the compositional boundaries along the solid solution
39 between Al and V^{3+} that are determined at $Y+Z(\text{V}_{1.5}\text{Al}_{5.5})$, corresponding to
40 $\text{Na}^Y(\text{V}_{1.5}\text{Al}_{1.5})^Z(\text{Al}_4\text{Mg}_2)\text{Si}_6\text{O}_{18}(\text{BO}_3)_3(\text{OH})_3\text{O}$, and $Y+Z(\text{V}_5\text{Al}_2)$, corresponding to
41 $\text{Na}^Y(\text{V}_3)^Z(\text{V}_2\text{Al}_2\text{Mg}_2)\text{Si}_6\text{O}_{18}(\text{BO}_3)_3(\text{OH})_3\text{O}$.

42

43

44

INTRODUCTION

45 The tourmaline supergroup minerals are widespread, occurring in sedimentary, igneous
46 and metamorphic rocks (Dutrow and Henry 2011). They are important indicator minerals that
47 can provide information on the compositional evolution of their host rocks, chiefly due to their
48 ability to incorporate a large number of elements (e.g., Novák et al. 2004; Agrosi et al. 2006;
49 Lussier et al. 2011a; Novák et al. 2011; van Hinsberg et al. 2011; Bačík et al. 2012). However,
50 the chemical composition of tourmalines is also controlled by short-range and long-range
51 constraints (e.g., Hawthorne 1996, 2002a; Bosi and Lucchesi 2007; Bosi 2010, 2011; Henry
52 and Dutrow 2011; Skogby et al. 2012; Bosi 2013) as well as by temperature (van Hinsberg and
53 Schumacher 2011). Tourmaline supergroup minerals are complex borosilicates and their
54 crystal structure and crystal chemistry have been extensively studied (e.g., Foit 1989;
55 Hawthorne and Henry 1999; Bosi and Lucchesi 2007; Lussier et al. 2008; Bosi 2008; Bosi et
56 al. 2010; Lussier et al. 2011b; Filip et al. 2012). In accordance with Henry et al. (2011), the
57 general formula of tourmaline may be written as: $\text{XY}_3\text{Z}_6\text{T}_6\text{O}_{18}(\text{BO}_3)_3\text{V}_3\text{W}$, where $X (\equiv [^9]X) =$
58 $\text{Na}^+, \text{K}^+, \text{Ca}^{2+}, \square$ (=vacancy); $Y (\equiv [^6]Y) = \text{Al}^{3+}, \text{Fe}^{3+}, \text{Cr}^{3+}, \text{V}^{3+}, \text{Mg}^{2+}, \text{Fe}^{2+}, \text{Mn}^{2+}, \text{Li}^+$; $Z (\equiv$
59 $[^6]Z) = \text{Al}^{3+}, \text{Fe}^{3+}, \text{Cr}^{3+}, \text{V}^{3+}, \text{Mg}^{2+}, \text{Fe}^{2+}$; $T (\equiv [^4]T) = \text{Si}^{4+}, \text{Al}^{3+}, \text{B}^{3+}$; $B (\equiv [^3]B) = \text{B}^{3+}$; $W (\equiv$
60 $[^3]O1) = \text{OH}^{1-}, \text{F}^{1-}, \text{O}^{2-}$; $V (\equiv [^3]O3) = \text{OH}^{1-}, \text{O}^{2-}$ and where, for example, T represents a group
61 of cations ($\text{Si}^{4+}, \text{Al}^{3+}, \text{B}^{3+}$) accommodated at the [4]-coordinated *T* sites. The dominance of
62 these ions at one or more sites of the structure gives rise to a range of distinct mineral species.

63 Recently, several new minerals of the tourmaline supergroup were approved by the
64 Commission on New Minerals, Nomenclature and Classification (CNMNC) of the

65 International Mineralogical Association (IMA). Among these are a number of oxy-tourmalines
66 related by complete solid solution in the Al^{3+} - Cr^{3+} - V^{3+} subsystem: oxy-dravite, end-member
67 formula $NaAl_3(Al_4Mg_2)(Si_6O_{18})(BO_3)_3(OH)_3O$ (IMA 2012-004a; Bosi and Skogby 2013),
68 oxy-chromium-dravite, $NaCr_3(Cr_4Mg_2)(Si_6O_{18})(BO_3)_3(OH)_3O$ (IMA 2011-097; Bosi et al.
69 2012a); oxy-vanadium-dravite, $NaV_3(V_4Mg_2)(Si_6O_{18})(BO_3)_3(OH)_3O$ (IMA 11-E; Bosi et al.
70 2013a).

71 A new species of oxy-tourmaline, vanadio-oxy-dravite, has been approved by the IMA-
72 CNMNC (proposal no. 2012-074). The holotype specimen (sample PR73) is deposited in the
73 collections of the Museum of Mineralogy, Earth Sciences Department, Sapienza University of
74 Rome, Italy, catalogue number 33068. A formal description of the new species vanadio-oxy-
75 dravite is presented here, including a full characterization of its physical, chemical and
76 structural properties.

77

78

79 OCCURRENCE, APPEARANCE AND PHYSICAL AND OPTICAL PROPERTIES

80 The crystals of vanadio-oxy-dravite are green and occur in metaquartzites in the
81 Pereval marble quarry, Sludyanka crystalline complex, Southern Baikal region, Russia
82 ($51^{\circ}37'N$ $103^{\circ}38'E$). The Pereval quarry is the type locality (see Bosi et al. 2012a for a more
83 detailed description) for natalyite, florensovite, kalininite, magnesiocoulsonite, oxy-vanadium-
84 dravite, oxy-chromium-dravite, vanadio-oxy-chromium-dravite, chromo-alumino-povondraite,
85 batisivite, oxyvanite and cuprokalininite. Minerals associated with the holotype specimen are:
86 quartz, Cr-V-bearing tremolite and muscovite-celadonite, diopside – kosmochlor – natalyite,
87 Cr-bearing goldmanite, esolaite – karelianite, dravite, V-bearing titanite and rutile, ilmenite,
88 oxyvanite – berdesinskiite, shreyerite, plagioclase, scapolite, zircon, pyrite and an unnamed
89 oxide of V, Cr, Ti, U and Nb, The host rocks (quartz-diopside) are Cr-V-bearing carbonate-
90 siliceous sediments, metamorphosed to granulite facies and partly diaphthorized (Salnikova et
91 al. 1998) to amphibolite facies (retrograde stage). Vanadio-oxy-chromium-dravite was formed
92 in the prograde stage (granulite facies). The crystals are euhedral, reaching up to 0.3 mm in
93 length, and may be chemically zoned (for details, see Figure 3 of Bosi et al. 2013a), but
94 homogeneous crystals also occur.

95 The morphology of vanadio-oxy-dravite consists of elongated $\{10\bar{1}0\}$ and $\{11\bar{2}0\}$
96 prisms terminated by a prominent $\{0001\}$ pedion and small, minor $\{10\bar{1}1\}$ pyramidal faces.

97 Crystals are green, with pale green streak, transparent and display vitreous luster. They are
98 brittle and show conchoidal fracture. The Mohs hardness is approximately 7½ (Reznitsky et al.
99 2001). The calculated density is 3.14 g/cm³. In transmitted light, vanadio-oxy-dravite is
100 pleochroic with O = yellow green and E = pale olive green. Vanadio-oxy-dravite is uniaxial
101 negative with refractive indices, measured by the immersion method using white light from a
102 tungsten source, of $\omega = 1.693(5)$, $\epsilon = 1.673(5)$. The mean index of refraction, density and
103 chemical composition lead to excellent compatibility indices ($1 - K_p/K_c = 0.026$) (Mandarino
104 1976, 1981)

105

106

107

METHODS

108 **Single-crystal structural refinement**

109 A representative fragment of the type specimen was selected for X-ray diffraction
110 measurements on a Bruker KAPPA APEX-II single-crystal diffractometer, at Sapienza
111 University of Rome (Earth Sciences Department), equipped with a CCD area detector (6.2 ×
112 6.2 cm² active detection area, 512 × 512 pixels) and a graphite crystal monochromator, using
113 MoK α radiation from a fine-focus sealed X-ray tube. The sample-to-detector distance was 4
114 cm. A total of ca. 3265 exposures (step = 0.2°, time/step = 20 s) covering a full reciprocal
115 sphere with a redundancy of about 8 was used. Final unit-cell parameters were refined by
116 means of the Bruker AXS SAINT program using reflections with $I > 10 \sigma(I)$ in the range $5^\circ <$
117 $2\theta < 73^\circ$. The intensity data were processed and corrected for Lorentz, polarization, and
118 background effects with the APEX2 software program of Bruker AXS. The data were
119 corrected for absorption using the multi-scan method (SADABS). The absorption correction
120 led to a significant improvement in R_{int} . No violations of $R3m$ symmetry were noted.

121 Structural refinement was done with the SHELXL-97 program (Sheldrick 2008).
122 Starting coordinates were taken from Bosi et al. (2004). Variable parameters were: scale
123 factor, extinction coefficient, atomic coordinates, site scattering values and atomic-
124 displacement factors. To obtain the best values of statistical indexes ($R1$, $wR2$), a fully ionized
125 scattering curve for O was used, whereas neutral scattering curves were used for the other
126 atoms. In detail, the occupancy of the X site was modeled by using the sodium scattering
127 factor, the Y site vanadium and magnesium scattering factors, and the Z site using vanadium
128 and aluminum factors. The T and B sites were modeled, respectively, with Si and B scattering
129 factors and with a fixed occupancy of 1, because refinement with unconstrained occupancies

130 showed no significant deviations from this value. Three full-matrix refinement cycles with
131 isotropic-displacement parameters for all atoms were followed by anisotropic cycles until
132 convergence was attained. No significant correlations over a value of 0.7 between the
133 parameters were observed at the end of refinement. Table 1 lists crystal data, data-collection
134 information and refinement details; Table 2 gives the fractional atomic coordinates and site
135 occupancies; Table 3 gives the displacement parameters; Table 4 gives selected bond
136 distances.

137

138 **X-ray powder diffraction**

139 Powder X-ray data were derived from the single-crystal structural refinement
140 since the available sample material was not sufficient for X-ray powder diffraction
141 measurements. Data are listed in Table 5.

142

143 **Electron-Microprobe analysis**

144 Electron-microprobe analyses of the crystal used for X-ray diffraction refinement were
145 obtained by wavelength-dispersive spectrometer (WDS mode) with a Cameca SX50
146 instrument at the “Istituto di Geologia Ambientale e Geoingegneria (Rome, Italy), CNR”,
147 operating at an accelerating potential of 15 kV and a sample current of 15 nA, 10 μm beam
148 diameter. Minerals and synthetic compounds were used as standards: wollastonite (Si, Ca),
149 magnetite (Fe), rutile (Ti), corundum (Al), vanadinite (V) fluorphlogopite (F), periclase (Mg),
150 jadeite (Na), K-feldspar (K), sphalerite (Zn), metallic Cr, Mn and Cu. The overlap corrections
151 and the PAP routine were applied (Pouchou and Pichoir 1991). The results (Table 6) represent
152 mean values of 10 spot analyses. In accord with the very low concentration of Li in dravitic
153 samples (e.g., Henry et al. 2011), the Li_2O content was assumed to be insignificant.
154 Manganese, Zn, Cu and F were below their respective detection limits (0.03 wt%) in the
155 studied sample.

156

157 **Infrared spectroscopy**

158 A homogeneous vanadio-oxy-dravite crystal was measured by Fourier transform
159 infrared (FTIR) absorption spectroscopy to characterize (OH) absorption bands in the
160 wavenumber range $2000\text{-}5000\text{ cm}^{-1}$ using a Bruker Equinox 55 spectrometer equipped with a
161 NIR source, a CaF_2 beam-splitter, a wire-grid polarizer and an InSb detector. Polarized spectra
162 with a resolution of 4 cm^{-1} were acquired parallel and perpendicular to the crystallographic c -

163 axis direction using a circular measurement area of 100 μm diameter on a 36 μm thick doubly-
164 polished crystal plate that had been oriented parallel the *c*-axis by morphology and optical
165 microscopy. As often observed, fundamental (OH) absorption bands polarized parallel to the
166 *c*-axis direction of tourmalines are exceptionally intense, and it was not possible to thin the
167 sample sufficiently to avoid off-scale absorption intensity for the strongest band (Fig. 1).

168

169 **Optical absorption spectroscopy**

170 Polarized, room-temperature optical-absorption spectra were recorded on the same 36
171 μm thick crystal platelet used for the FTIR measurements. The spectra were measured in the
172 range 270-1100 nm ($37037\text{-}9091\text{ cm}^{-1}$) at a resolution of 1 nm using an AVASPEC-
173 ULS2048X16 spectrometer attached via a 400 μm UV optical fiber to a Zeiss Axiotron UV-
174 microscope. A 75 W Xenon arc lamp served as illuminating source and Zeiss Ultrafluar 10x
175 lenses served as objective and condenser. A UV-quality Glan-Thompson prism with a working
176 range from 250 to 2700 nm ($40000\text{ to }3704\text{ cm}^{-1}$) was used as polarizer. The size of the
177 circular measure aperture was 64 μm in diameter. The wavelength scale of the spectrometer
178 was calibrated against Ho_2O_3 doped and $\text{Pr}_2\text{O}_3/\text{Nd}_2\text{O}_3$ doped standards (Hellma glass filters
179 666F1 and 666F7) with an accuracy better than 15 cm^{-1} in the wavelength range 300-1100 nm.
180 Recorded spectra were fitted using the Jandel PeakFit 4.12 software assuming Gaussian peak
181 shapes.

182

183 **RESULTS AND DISCUSSION**

184 **General comment**

185 The present crystal-structure refinement and electron-microprobe analyses were
186 obtained from the same single crystal. However, complementary optical and spectroscopic
187 data were recorded from coexisting crystals. Small differences in composition are likely to
188 occur between these crystals.

189

190 **Determination of atomic proportions**

191 In agreement with the structural-refinement results, the boron content was assumed to
192 be stoichiometric in the vanadio-oxy-dravite sample ($\text{B}^{3+} = 3.00\text{ apfu}$). Both the site-scattering
193 results and the bond lengths of *B* and *T* are consistent with the *B* site fully occupied by boron
194 and no amount of B^{3+} at the *T* site (e.g., Hawthorne 1996; Bosi and Lucchesi 2007). In line

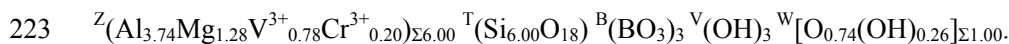
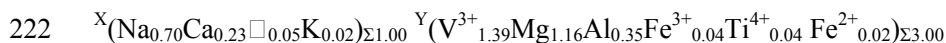
195 with the optical absorption results, which show the occurrence of both Fe^{2+} and Fe^{3+} (see
196 below), the Fe contents were calculated on the basis of $\text{Fe}^{3+}/\Sigma\text{Fe} = 0.68$, measured by
197 Mössbauer spectroscopy (Bosi et al. 2013b) for a Fe-bearing chromo-alumino-povondraite
198 coming from the same locality as the present sample. Note that due to the relatively low
199 concentrations of Fe, uncertainty on its oxidation state has little influence on the overall charge
200 calculations. The (OH) content can then be calculated by charge balance with the assumption
201 $T + Y + Z = 15.00$. The atomic proportions were calculated on this assumption (Table 6). The
202 excellent match between the number of electrons per formula unit (epfu) derived from
203 chemical and structural analysis supports this procedure, respectively: 251.2 epfu and 251.3
204 epfu.

205

206 **Site populations**

207 The anion site populations in the studied sample follow the general preference
208 suggested for tourmaline (e.g., Grice and Ercit 1993; Henry et al. 2011): the O3 site (V
209 position in the general formula) is occupied by (OH), and the O1 site (W position in the
210 general formula) is occupied by O^{2-} and (OH). The cation distribution at the T, Y and Z sites
211 was optimized by using a quadratic program to minimize the residuals between calculated and
212 observed data (based on the chemical and structural analysis). Site-scattering values,
213 octahedral and tetrahedral mean bond-distances (i.e., $\langle Y-O \rangle$, $\langle Z-O \rangle$ and $\langle T-O \rangle$) were
214 calculated as the linear contribution of each cation multiplied by its ideal bond-distance (Table
215 7). More details about the ideal distances as well as about the optimization procedure may be
216 found in Bosi et al. (2004) and Bosi and Lucchesi (2004; 2007). The robustness of this
217 approach was confirmed by another optimization procedure (Wright et al. 2000), which led to
218 very similar cation distributions (Table 7). This result represents another example of
219 convergence of these two procedures to similar solutions for tourmaline (e.g., Bosi and
220 Lucchesi 2007; Filip et al. 2012; Bosi et al. 2012a, 2013a).

221 The final structural formulae are as follows:



224 The bond-valence analysis is consistent with the optimized structural formulae. Bond-valence
225 calculations, using the formula and bond-valence parameters from Brown and Altermatt
226 (1985), are reported in Table 8.

227

228 **Name and crystal chemistry**

229 The chemical composition of sample PR73 is consistent with tourmalines belonging to
230 the alkali group, oxy-subgroup 3 (Henry et al. 2011). They are Na-dominant at the X site,
231 oxygen-dominant at W with $O^{2-} > (OH+F)^{1-}$. As V^{3+} is the dominant cation at Y and Al^{3+} is the
232 dominant cation at Z, its end-member composition may be represented as
233 $NaV_3(Al_4Mg_2)Si_6O_{18}(BO_3)_3(OH)_3O$. This is in accord with the dominant-valency rule (Hatert
234 and Burke 2008) for which the dominant ion of the dominant valency at one site becomes the
235 basis for naming the species. As no tourmalines have yet been reported with V^{3+} - and Al^{3+} -
236 dominant at Y and Z, respectively, this tourmaline can be classified as a new species. The
237 closest end-member composition of a valid tourmaline species is that of oxy-dravite. The
238 name vanadio-oxy-dravite may hence be assigned for the chemical composition, following
239 Henry et al. (2011). The prefix *vanadio* represents the substitution of $3V^{3+}$ for 3Al in the root
240 composition of oxy-dravite.

241 Although there exists a significant degree of V^{3+} , Al and Mg disorder over the Y and Z
242 sites, the structural formula of sample PR73 indicates a clear preference of V^{3+} for the Y site
243 and Al for the Z site, while Mg shows only a slight preference for the Z site. Chromium, on the
244 other hand, seems completely ordered at the Z site. The O1 site is dominated by O^{2-} with a
245 relatively minor concentration of (OH). The presence of only minor concentrations of (OH) at
246 O1 (~ 0.26 apfu) are consistent with both the observation of weak absorption bands at 3761
247 and 3732 cm^{-1} in the infrared spectrum (Fig. 1), i.e. the area typically ascribed to the O1 site
248 (see below), and the equation proposed by Bosi (2013) to estimate the (OH) contents in
249 tourmaline: $^W(OH) = [2 - 1.01 \cdot BVS(O1) - 0.21 - F] = 0.27$ apfu.

250

251 **End-member formula**

252 Although the amount of Mg at Z is larger than that at Y (1.28 and 1.16 apfu,
253 respectively), the formula of vanadio-oxy-dravite may also be approximated as
254 $Na^Y(V^{3+}_2Mg)^Z(Al_4MgV^{3+})(Si_6O_{18})(BO_3)_3(OH)_3O$. Such a formula could represent the
255 structural formula for vanadio-oxy-dravite, but is not an end-member formula. In fact, this
256 composition has multiple cations at more than one site (i.e., V^{3+} and Mg over Y and Z), and
257 hence is inconsistent with the characteristics of an ordered end-member formula as defined by
258 Hawthorne (2002b). The most ordered site allocation of V^{3+} , Al and Mg consistent with the
259 empirical formula and the end-member definition is $Na^Y(V_3)^Z(Al_4Mg_2)(Si_6O_{18})(BO_3)_3(OH)_3O$.

260 Note that the difference between these two formulae is solely in V^{3+} -Mg order-disorder; no
261 difference occurs in chemical composition.

262

263 **Infrared spectroscopy**

264 Spectra recorded in polarized mode perpendicular and parallel to the crystallographic **c**
265 axis show an intense broad band around 3550 cm^{-1} and two weaker bands at 3732 and 3761
266 cm^{-1} , all strongly polarized in the **c** direction (Fig. 1). As it was not possible to thin the sample
267 sufficiently to avoid off-scale absorption for the main band, any possible fine structure cannot
268 be discerned. However, in line with previous studies (Bosi et al. 2012b; Bosi et al. 2013b), the
269 band can be related to the local arrangement ($^YV^{3+}Z^R$)-O3, i.e., to the occurrence of (OH)
270 at the V position of the tourmaline general formula (O3 site in the structure). The two weaker
271 bands at ca. 3732 and 3761 cm^{-1} are consistent with the minor concentrations of (OH) (ca. 0.3
272 apfu) assigned to the W position (O1 site in the structure), and may be related to the local
273 arrangements $^Y(\text{Mg Mg Mg})$ and $^Y(\text{Mg Mg R})$ (cf. Gonzalez-Carreño et al. 1988; Bosi et al.
274 2012b; Bosi et al. 2013b).

275

276

277 **Optical-absorption spectroscopy**

278 The optical spectra of vanadio-oxy-dravite show two broad absorption bands at ca. 432
279 and 609 nm, superimposed on an intense UV absorption edge (Fig. 3). These absorption bands
280 are ascribed to spin-allowed *d-d* transitions in octahedrally coordinated V^{3+} , in accord with
281 similar bands observed for vanadio-oxy-chromium-dravite (Bosi et al. 2012c) at ca. 440 and
282 610 nm. In addition to the dominant V^{3+} -bands, two broad but weak absorption bands at ca.
283 765 and 1100 nm are observed in the **E||a**-spectrum. They are in accord with previous studies
284 on the optical spectra of tourmaline (e.g., Smith 1978; Taran et al. 1993; Mattson and
285 Rossman 1987) and are ascribed to electronic transitions in Fe^{2+} - Fe^{3+} pairs. Consequently, the
286 appearance of these absorption bands suggests that a small fraction of the total iron in the
287 present sample occurs in the divalent state.

288

289

290 **COMPOSITIONAL BOUNDARIES OF VANADIO-OXY-DRAVITE**

291 The plot of the Z- and Y-site cations in the ternary diagram for the Al-Cr- V^{3+}
292 subsystem show, of course, that vanadio-oxy-dravite is Z Al-dominant and $^YV^{3+}$ -dominant.

293 More interesting, however, is the triangular plot in terms of Al-Cr-V³⁺ at Y and Z, showing that
294 vanadio-oxy-dravite can be either Al-dominant or V³⁺-dominant (Fig. 3). This latter plot type
295 displays the occurrence of three end-members along the full solid solution between the Al³⁺
296 and V³⁺ apices: oxy-dravite, vanadio-oxy-dravite and oxy-vanadium-dravite. These end-
297 members are related by the substitution V³⁺ ↔ Al³⁺ at the Y position (vanadio-oxy-dravite ↔
298 oxy-dravite) and V³⁺ ↔ Al³⁺ at the Z position (oxy-vanadium-dravite ↔ vanadio-oxy-dravite),
299 while their compositional boundaries are at: (1) ^{Y+Z}(V₅Al₂), corresponding to
300 Na^Y(V₃)^Z(V₂Al₂Mg₂)Si₆O₁₈(BO₃)₃(OH)₃O; (2) ^{Y+Z}(V_{1.5}Al_{5.5}), corresponding to
301 Na^Y(V_{1.5}Al_{1.5})^Z(Al₄Mg₂)Si₆O₁₈(BO₃)₃(OH)₃O. Consequently, oxy-dravite is characterized by
302 V³⁺ contents less than 1.5 apfu, vanadio-oxy-dravite is characterized by V³⁺ contents between
303 5 and 1.5 apfu, and oxy-vanadium-dravite is characterized by V³⁺ contents larger than 5 apfu.

304 The discovery of the new mineral vanadio-oxy-dravite provides new information on
305 the crystal chemistry of the tourmaline supergroup. The current chemical data supports
306 complete exchange of V³⁺, Cr³⁺ and Al in species of the tourmaline supergroup (Reznitsky et
307 al. 2001; Bosi et al. 2004, 2013a,b), and it shows that vanadio-oxy-dravite can be either V³⁺-
308 dominant or Al-dominant.

309

310

311

ACKNOWLEDGMENTS

312 Chemical analyses were done with the kind assistance of M. Serracino to whom the
313 authors express their gratitude. L. Reznitskii was supported by a grant from the Russian
314 Foundation for Basic Research (project 13-05-00258). We thank the reviewers Darrel Henry
315 and Frank C. Hawthorne for useful suggestions that improved the manuscript. The manuscript
316 handling by Daniel Harlov is acknowledged.

317

318

319

REFERENCES CITED

- 320 Agrosi, G., Bosi, F., Lucchesi, S., Melchiorre, G., and Scandale, E. (2006) Mn-tourmaline
321 crystals from island of Elba (Italy): Growth history and growth marks. American
322 Mineralogist, 91, 944-952.
- 323 Bačík P., Méres Š., Uher P. (2011) Vanadium-bearing tourmaline in metacherts from
324 Chvojnica, Slovak Republic: crystal chemistry and multistage evolution. Canadian
325 Mineralogist, 49, 195-206.

- 326 Bačík, P., Uher, P., Ertl, A., Jonsson, E., Nysten, P., Kanický, V., and Vaculovič, T. (2012)
327 Zoned REE Enriched Dravite from a Granitic Pegmatite in Forshammar Bergslagen
328 Province, Sweden an EMPA, XRD and LA-ICP-MS study. Canadian Mineralogist, 50,
329 825-841.
- 330 Bosi, F. (2008) Disordering of Fe²⁺ over octahedrally coordinated sites of tourmaline.
331 American Mineralogist, 93, 1647-1653.
- 332 Bosi, F. (2010) Octahedrally coordinated vacancies in tourmaline: a theoretical approach.
333 Mineralogical Magazine, 74, 1037-1044.
- 334 Bosi, F. (2011) Stereochemical constraints in tourmaline: from a short-range to a long-range
335 structure. Canadian Mineralogist, 49, 17-27.
- 336 Bosi, F. (2013) Bond-valence constraints around the O1 site of tourmaline. Mineralogical
337 Magazine, 77, 343-351.
- 338 Bosi, F. and Lucchesi, S. (2004) Crystal chemistry of the schorl-dravite series. European
339 Journal of Mineralogy, 16, 335-344.
- 340 Bosi, F. and Lucchesi, S. (2007) Crystal chemical relationships in the tourmaline group:
341 structural constraints on chemical variability. American Mineralogist, 92, 1054-1063.
- 342 Bosi, F. and Skogby, H. (2013) Oxy-dravite, Na(Al₂Mg)(Al₅Mg)(Si₆O₁₈)(BO₃)₃(OH)₃O, a new
343 mineral species of the tourmaline supergroup. American Mineralogist, 98,
344 dx.doi.org/10.2138/am.2013.4441.
- 345 Bosi F., Lucchesi, S., and Reznitskii, L. (2004) Crystal chemistry of the dravite-chromdravite
346 series. European Journal of Mineralogy, 16, 345-352.
- 347 Bosi, F., Balić-Žunić, T., and Surour, A.A., (2010) Crystal structure analysis of four
348 tourmalines from the Cleopatra's Mines (Egypt) and Jabal Zalm (Saudi Arabia), and the
349 role of Al in the tourmaline group. American Mineralogist, 95, 510-518.
- 350 Bosi, F., Reznitskii, L., and Skogby, H. (2012a) Oxy-chromium-dravite,
351 NaCr₃(Cr₄Mg₂)(Si₆O₁₈)(BO₃)₃(OH)₃O, a new mineral species of the tourmaline
352 supergroup. American Mineralogist, 97, 2024-2030.
- 353 Bosi, F., Skogby, H., Agrosi, G., and Scandale, E. (2012b) Tsilaisite,
354 NaMn₃Al₆(Si₆O₁₈)(BO₃)₃(OH)₃OH, a new mineral species of the tourmaline supergroup
355 from Grotta d'Oggi, San Pietro in Campo, island of Elba, Italy. American Mineralogist,
356 97, 989-994.

- 357 Bosi, F., Reznitskii, L., Skogby, H., and Hålenius, U. (2012c) Vanadio-oxy-chromium-dravite
358 IMA 2012-034. CNMNC Newsletter No. 14, October 2012, page 1286; Mineralogical
359 Magazine, 76, 1281-1288.
- 360 Bosi, F., Reznitskii, L., and Sklyarov, E.V. (2013a) Oxy-vanadium-dravite,
361 $\text{NaV}_3(\text{V}_4\text{Mg}_2)(\text{Si}_6\text{O}_{18})(\text{BO}_3)_3(\text{OH})_3\text{O}$: crystal structure and redefinition of the
362 “vanadium-dravite” tourmaline. American Mineralogist. 98, 501-505.
- 363 Bosi, F., Skogby, H., Hålenius, U., and Reznitskii, L. (2013b) Crystallographic and
364 spectroscopic characterization of Fe-bearing chromo-alumino-povondraite and its
365 relations with oxy-chromium-dravite and oxy-dravite. American Mineralogist, 98,
366 dx.doi.org/10.2138/am.2013.4447.
- 367 Brown, I.D. and Altermatt, D. (1985) Bond-valence parameters obtained from a systematic
368 analysis of the Inorganic Crystal Structure Database. Acta Crystallographica, B41, 244–
369 247.
- 370 Dutrow, B.L. and Henry, D.J. (2011) Tourmaline: A geologic DVD. Elements, 7(5), 301-306.
- 371 Filip, J., Bosi, F., Novák, M., Skogby, H., Tuček, J., Čuda, J., and Wildner, M. (2012) Redox
372 processes of iron in the tourmaline structure: example of the high-temperature treatment
373 of Fe^{3+} -rich schorl. Geochimica et Cosmochimica Acta, 86, 239-256.
- 374 Foit, F.F. Jr. (1989) Crystal chemistry of alkali-deficient schorl and tourmaline structural
375 relationships. American Mineralogist, 74, 422-431.
- 376 Gonzalez-Carreño, T., Fernandez, M. and Sanz, J. (1988) Infrared and electron microprobe
377 analysis in tourmalines. Physics and Chemistry of Minerals, 15, 452-460.
- 378 Grice, J.D. and Ercit, T.S. (1993) Ordering of Fe and Mg in the tourmaline crystal structure:
379 the correct formula. Neues Jahrbuch für Mineralogie, Abhandlungen, 165, 245-266.
- 380 Hatert, F. and Burke, E.A.J. (2008) The IMA-CNMNC dominant-constituent rule revisited and
381 extended. Canadian Mineralogist, 46, 717-728.
- 382 Hawthorne, F.C. (1996) Structural mechanisms for light-element variations in tourmaline.
383 Canadian Mineralogist, 34, 123-132.
- 384 Hawthorne, F. C. (2002a) Bond-valence constraints on the chemical composition of
385 tourmaline. Canadian Mineralogist, 40, 789-797.
- 386 Hawthorne, F.C. (2002b) The use of end-member charge-arrangements in defining new
387 mineral species and heterovalent substitutions in complex minerals. Canadian
388 Mineralogist, 40, 699-710

- 389 Hawthorne, F.C. and Henry, D. (1999) Classification of the minerals of the tourmaline group.
390 European Journal of Mineralogy, 11, 201-215.
- 391 Henry, D.J. and Dutrow, B.L. (2011) The incorporation of fluorine in tourmaline: Internal
392 crystallographic controls or external environmental influences? Canadian Mineralogist,
393 49, 41-56.
- 394 Henry, D.J., Novák, M., Hawthorne, F.C., Ertl, A., Dutrow, B., Uher, P., and Pezzotta, F.
395 (2011) Nomenclature of the tourmaline supergroup minerals. American Mineralogist, 96,
396 895-913.
- 397 Lussier, A.J., Aguiar, P.M., Michaelis, V.K., Kroeker, S., Herwig, S., Abdu, Y., and
398 Hawthorne, F.C. (2008) Mushroom elbaite from the Kat Chay mine, Momeik, near
399 Mogok, Myanmar: I. Crystal chemistry by SREF, EMPA, MAS NMR and Mössbauer
400 spectroscopy. Mineralogical Magazine, 72, 747-761.
- 401 Lussier, A.J., Hawthorne, F.C., Aguiar, P.M., Michaelis, V.K., and Kroeker, S. (2011a)
402 Elbaite-liddicoatite from Black Rapids glacier, Alaska. Periodico di Mineralogia, 80, 57-
403 73.
- 404 Lussier, A.J., Abdu, Y. Hawthorne, F.C., Michaelis, V.K., Aguiar, P.M., and Kroeker, S.
405 (2011b) Oscillatory zoned liddicoatite from Anjanabonoina, central Madagascar. I.
406 Crystal chemistry and structure by SREF and ^{11}B and ^{27}Al MAS NMR spectroscopy.
407 Canadian Mineralogist, 49, 63-88.
- 408 Mandarino, J.A. (1976) The Gladstone-Dale relationship. Part I: derivation of new constants.
409 Canadian Mineralogist, 14, 498-502.
- 410 Mandarino, J.A. (1981) The Gladstone-Dale relationship. Part IV: the compatibility concept
411 and its application. Canadian Mineralogist, 19, 441-450.
- 412 Mattson, S.M. and Rossman, G.R. (1987) Fe^{2+} - Fe^{3+} interactions in tourmaline. Physics and
413 Chemistry of Minerals, 14, 163-171.
- 414 Novák, M., Povondra, P., and Selway, J.B. (2004) Schorl-oxy-schorl to dravite-oxy-dravite
415 tourmaline from granitic pegmatites; examples from the Moldanubicum, Czech
416 Republic. European Journal of Mineralogy, 16, 323-333.
- 417 Novák M., Škoda P., Filip J., Macek I., and Vaculovič T. (2011) Compositional trends in
418 tourmaline from intragranitic NYF pegmatites of the Třebíč Pluton, Czech Republic;
419 electron microprobe, Mössbauer and LA-ICP-MS study. Canadian Mineralogist, 49,
420 359-380.

- 421 Pouchou, J.L. and Pichoir, F. (1991) Quantitative analysis of homogeneous or stratified
422 microvolumes applying the model "PAP." In K.F.J. Heinrich and D.E. Newbury, Eds.,
423 Electron Probe Quantitation, p. 31–75. Plenum, New York.
- 424 Reznitsky, L.Z., Sklyarov, E.V., Ushchapovskaya, Z.V., Nartova, N.V., Kashaev, A.A.,
425 Karmanov, N.S., Kanakin, S.V., Smolin, A.S., and Nekrosova, E.A. (2001)
426 Vanadiumdravite, $\text{NaMg}_3\text{V}_6[\text{Si}_6\text{O}_{18}][\text{BO}_3]_3(\text{OH})_4$, a new mineral of the tourmaline
427 group. *Zapiski Vsesoyuznogo Mineralogicheskogo Obshchestva*, 130, 59-72 (in
428 Russian).
- 429 Salnikova, E.B., Sergeev, S.A., Kotov, A.B., Yakovleva, S.Z., Steiger, R.H., Reznitskiy, L.Z.,
430 and Vasil'ev, E.P. (1998) U-Pb zircon dating of granulite metamorphism in the
431 Slyudyanskiy complex, Eastern Siberia. *Gondwana Research*, 1, 195–205.
- 432 Sheldrick, G.M. (2008) A short history of SHELX. *Acta Crystallographica*, A64, 112-122.
- 433 Smith, G. (1978) A reassessment of the role of iron in the 5,000-30,000 cm^{-1} region of the
434 electronic absorption spectra of tourmaline. *Physics and Chemistry of Minerals*, 3, 343-
435 373.
- 436 Skogby, H., Bosi, F., and Lazor, P. (2012) Short-range order in tourmaline: a vibrational
437 spectroscopic approach to elbaite. *Physics and Chemistry of Minerals*, 39, 811-816.
- 438 Taran, M.N., Lebedev, A.S., and Platonov, A.N. (1993) Optical absorption spectroscopy of
439 synthetic tourmalines. *Physics and Chemistry of Minerals*, 20, 209-220.
- 440 van Hinsberg, V.J. and Schumacher, J.C. (2011) Tourmaline as a petrogenetic indicator
441 mineral in the Haut-Allier metamorphic suite, Massif Central, France. *Canadian*
442 *Mineralogist*, 49, 177-194.
- 443 van Hinsberg, V.J., Henry, D.J., and Marschall, H.R. (2011) Tourmaline: an ideal indicator of
444 its host environment. *Canadian Mineralogist*, 49, 1-16.
- 445 Wright, S.E., Foley, J.A., and Hughes, J.M. (2000) Optimization of site occupancies in
446 minerals using quadratic programming. *American Mineralogist*, 85, 524-531.
- 447

448

449

LIST OF TABLES

450 **TABLE 1.** Single-crystal X-ray diffraction data details for vanadio-oxy-dravite.

451 **TABLE 2.** Fractional atom coordinates and site occupancy for vanadio-oxy-dravite.

452 **TABLE 3.** Displacement parameters (\AA^2) for vanadio-oxy-dravite.

453 **TABLE 4.** Selected bond distances (\AA) for vanadio-oxy-dravite.

454 **TABLE 5.** Simulated X-ray powder diffraction data for vanadio-oxy-dravite.

455 **TABLE 6.** Chemical composition of vanadio-oxy-dravite.

456 **TABLE 7.** Cation site populations (apfu), mean atomic number and mean bond distances (\AA)
457 for vanadio-oxy-dravite.

458 **TABLE 8.** Bond valence calculations (valence unit) for vanadio-oxy-dravite.

459 **TABLE 9.** Comparative data for oxy-dravite, vanadio-oxy-dravite and oxy-vanadium-dravite.

460

461

462

LIST OF FIGURES AND FIGURE CAPTIONS

463 **FIGURE 1.** Polarized FTIR absorption spectra in the (OH)-stretching region of vanadio-oxy-
464 dravite, vertically offset for clarity. Sample thickness 36 μm . The main band
465 around 3550 cm^{-1} is truncated in the *c* direction due to excessive absorption.

466 **FIGURE 2.** Polarized electronic absorption spectra for vanadio-oxy-dravite (sample PR73).

467 **FIGURE 3.** Ternary diagram in terms of Al-V-Cr at the *Y* + *Z* sites for oxy-tourmalines. Black
468 circle: present sample. Open circles: V^{3+} -bearing oxy-dravite samples with $\text{V}^{3+} >$
469 0.20 apfu (Bačík et al. 2011); and sample N825, oxy-vanadium-dravite (Bosi et al.
470 2013a); black crosses = vanadio-oxy-dravite samples from Sludyanka (Reznitsky et
471 al. 2001).

472

473

Table 1. Single-crystal X-ray diffraction data: details for vanadio-oxy-dravite

Sample	PR73
Crystal size (mm)	0.10 × 0.16 × 0.24
<i>a</i> (Å)	16.0273(3)
<i>c</i> (Å)	7.2833(1)
<i>V</i> (Å ³)	1620.24(5)
Range for data collection, 2θ (°)	5 - 73
Reciprocal space range <i>hkl</i>	-21 ≤ <i>h</i> ≤ 25 -23 ≤ <i>k</i> ≤ 26 -12 ≤ <i>l</i> ≤ 11
Total number of frames	3265
Set of measured reflections	7988
Unique reflections, <i>R</i> _{int} (%)	1800, 2.10
Redundancy	8
Absorption correction method	SADABS
Refinement method	Full-matrix least-squares on <i>F</i> ²
Structural refinement program	SHELXL-97
Extinction coefficient	0.00007(1)
Flack parameter	0.06(2)
<i>wR</i> ₂ (%)	3.81
<i>R</i> ₁ (%) all data	1.70
<i>R</i> ₁ (%) for <i>I</i> > 2σ(<i>I</i>)	1.65
GooF	1.060
Largest diff. peak and hole (±e ⁻ /Å ³)	0.40 and -0.30

Notes: *R*_{int} = merging residual value; *R*₁ = discrepancy index, calculated from *F*-data; *wR*₂ = weighted discrepancy index, calculated from *F*²-data; GooF = goodness of fit; Diff. Peaks = maximum and minimum residual electron density. Radiation, MoKα = 0.71073 Å. Data collection temperature = 293 K. Space group *R*3*m*; *Z* = 3.

TABLE 2. Fractional atom coordinates and site occupancy for vanadio-oxy-dravite

Site	x	y	z	Site occupancy
X	0	0	0.22772(15)	Na _{1.137(6)}
Y	0.12347(2)	0.061737(12)	0.63625(6)	V _{0.513(4)} Mg _{0.487(4)}
Z	0.29820(2)	0.26190(2)	0.61148(6)	Al _{0.852(3)} V _{0.148(3)}
B	0.11004(6)	0.22007(12)	0.4539(2)	B _{1.00}
T	0.191020(18)	0.189344(19)	0.000	Si _{1.00}
O1 (≡W)	0	0	0.7691(3)	O _{1.00}
O2	0.06078(4)	0.12157(8)	0.48340(16)	O _{1.00}
O3 (≡V)	0.26119(9)	0.13059(4)	0.51120(17)	O _{1.00}
O4	0.09258(4)	0.18516(8)	0.07085(16)	O _{1.00}
O5	0.18236(8)	0.09118(4)	0.09011(16)	O _{1.00}
O6	0.19403(5)	0.18472(5)	0.77971(12)	O _{1.00}
O7	0.28367(5)	0.28332(5)	0.07786(11)	O _{1.00}
O8	0.20860(5)	0.26946(6)	0.44063(12)	O _{1.00}
H3	0.2565(16)	0.1283(8)	0.393(3)	H _{1.00}

TABLE 3. Displacement parameters (\AA^2) for vanadio-oxy-dravite

Site	U^{11}	U^{22}	U^{33}	U^{23}	U^{13}	U^{12}	$U_{\text{eq}}/U_{\text{iso}}^*$
X	0.0149(4)	0.0149(4)	0.0158(5)	0.000	0	0.00743(18)	0.0152(3)
Y	0.00704(16)	0.00604(13)	0.00951(17)	-0.00095(5)	-0.00189(10)	0.00352(8)	0.00742(10)
Z	0.00619(13)	0.00663(13)	0.00729(12)	0.00037(9)	-0.00002(9)	0.00314(10)	0.00673(8)
B	0.0075(4)	0.0083(6)	0.0088(6)	0.0008(5)	0.0004(2)	0.0041(3)	0.0081(3)
T	0.00521(12)	0.00494(11)	0.00708(12)	-0.00055(9)	-0.00045(9)	0.00252(9)	0.00575(6)
O1	0.0104(5)	0.0104(5)	0.0077(8)	0.000	0	0.0052(2)	0.0095(3)
O2	0.0088(3)	0.0052(4)	0.0120(5)	0.0014(3)	0.00071(17)	0.0026(2)	0.0091(2)
O3	0.0179(5)	0.0139(4)	0.0061(5)	0.00053(19)	0.0011(4)	0.0089(3)	0.0122(2)
O4	0.0084(3)	0.0162(5)	0.0094(5)	-0.0009(4)	-0.00045(19)	0.0081(3)	0.0104(2)
O5	0.0158(5)	0.0078(3)	0.0097(5)	0.00071(19)	0.0014(4)	0.0079(3)	0.01019(19)
O6	0.0102(3)	0.0085(3)	0.0068(3)	-0.0014(2)	-0.0008(2)	0.0053(3)	0.00825(13)
O7	0.0079(3)	0.0069(3)	0.0101(3)	-0.0008(2)	-0.0028(3)	0.0014(3)	0.00929(14)
O8	0.0045(3)	0.0097(3)	0.0178(4)	0.0025(3)	0.0009(3)	0.0029(3)	0.01094(15)
H3							0.018*

Notes: Equivalent (U_{eq}) and isotropic (U_{iso}) displacement parameters; H-atom was constrained to have a U_{iso} 1.5 times the U_{eq} value of the O3 oxygen.

TABLE 4. Selected bond distances (Å) for vanadio-oxy-dravite

B-O2	1.384(2)	Y-O1	1.9682(10)
B-O8 ^A (× 2)	1.3715(11)	Y-O2 ^B (× 2)	2.0327(8)
<B-O>	1.376	Y-O3	2.1174(12)
		Y-O6 ^C (× 2)	2.0066(8)
T-O4	1.6292(5)	<Y-O>	2.027
T-O5	1.6453(5)		
T-O7	1.5995(7)	Z-O3	2.0164(6)
T*-O6	1.6080(9)	Z-O6	1.9374(8)
<T-O>	1.620	Z-O8 ^E	1.9178(8)
		Z-O7 ^E	1.9349(8)
X-O2 ^{B,F} (× 3)	2.5129(13)	Z-O7 ^D	1.9836(8)
X-O4 ^{B,F} (× 3)	2.8126(13)	Z-O8	1.9492(8)
X-O5 ^{B,F} (× 3)	2.7223(12)	<Z-O>	1.957
<X-O>	2.683	O3-H	0.86(2)

Notes: Standard uncertainty in parentheses. Superscript letters: A = ($y - x$, y , z); B = ($y - x$, $-x$, z); C = (x , $x - y$, z); D = ($y - x + 1/3$, $-x + 2/3$, $z + 2/3$); E = ($-y + 2/3$, $x - y + 1/3$, $z + 1/3$); F = ($-y$, $x - y$, z). Transformations relate coordinates to those of Table 2.

* Positioned in adjacent unit cell.

TABLE 5. Simulated X-ray powder diffraction data for vanadio-oxy-dravite ($\lambda = 1.5418 \text{ \AA}$)

$I_{\text{calc}} > 9$ (%)	d_{calc} (Å)	h	k	l
37	6.4467	1	0	1
19	5.0153	0	2	1
19	4.6185	3	0	0
52	4.2606	2	1	1
66	4.0041	2	2	0
47	3.5221	0	1	2
10	3.0317	4	1	0
67	2.9928	1	2	2
100	2.5958	0	5	1
15	2.3970	2	3	2
15	2.3594	5	1	1
13	2.2091	5	0	2
12	2.1500	0	3	3
11	2.0763	2	2	3
43	2.0573	1	5	2
28	1.9340	3	4	2
20	1.6756	0	6	3
13	1.6520	2	7	1
17	1.6025	5	5	0
15	1.5226	0	5	4
15	1.4704	5	1	4
10	1.4232	4	3	4

Notes: I = calculated intensity, d = calculated interplanar spacing; hkl = reflection indices.

TABLE 6. Chemical composition of vanadio-oxy-dravite

	Weight %		apfu
SiO ₂	35.34(17)	Si	6.00(3)
TiO ₂	0.29(4)	Ti ⁴⁺	0.037(5)
B ₂ O ₃ *	10.23	B	3.00
Al ₂ O ₃	20.36(37)	Al	4.08(6)
Cr ₂ O ₃	1.48(28)	Cr ³⁺	0.20(4)
V ₂ O ₃	15.97(39)	V ³⁺	2.18(5)
Fe ₂ O ₃ [†]	0.34	Fe ³⁺	0.044(4)
FeO [†]	0.15	Fe ²⁺	0.021(3)
MgO	9.65(10)	Mg	2.44(3)
CaO	1.24(7)	Ca	0.23(1)
Na ₂ O	2.11(6)	Na	0.70(2)
K ₂ O	0.09(1)	K	0.019(2)
H ₂ O*	2.86	OH	3.26
Total	100.12		

* Calculated by stoichiometry.

† Calculated as Fe³⁺/ΣFe ratio = 0.68 (see text); measured FeO = 0.45(4).

Notes: Errors for oxides are standard deviations (in brackets) of 10 spot analyses. Standard errors for the atomic proportions (in brackets) were calculated by error-propagation theory; apfu = atoms per formula unit.

TABLE 7. Cation site populations (apfu), mean atomic numbers and mean bond lengths (Å) for vanadio-oxy-dravite

Site	Site population	Mean atomic number		Mean bond length	
		refined	calculated	refined	calculated*
X	0.70 Na + 0.23 Ca + 0.05 □ + 0.02 K	12.51(8)	12.52		
Y	1.39 V ³⁺ + 1.16 Mg + 0.35 Al + 0.04 Fe ³⁺ + 0.04 Ti ⁴⁺ + 0.02 Fe ²⁺ (1.39 V ³⁺ + 1.20 Mg + 0.30 Al + 0.04 Fe ³⁺ + 0.04 Ti ⁴⁺ + 0.02 Fe ²⁺) [†]	17.64(7)	17.65	2.027	2.032
Z	3.73 Al + 1.28 Mg + 0.78 V ³⁺ + 0.20 Cr ³⁺ (3.77 Al + 1.24 Mg + 0.79 V ³⁺ + 0.20 Cr ³⁺) [†]	14.48(4)	14.46	1.957	1.955
T	6.00 Si	14 [‡]	14.00	1.620	1.620
B	3 B	5 [‡]	5		

Notes: apfu = atoms per formula unit;

* Calculated using the ionic radii of Bosi and Lucchesi (2007).

[†] Site populations optimized by the procedure of Wright et al. (2000).

[‡] Fixed in the final stages of refinement

TABLE 8. Bond-valence calculations (valence unit) for vanadio-oxy-dravite.

Site	X	Y	Z	T	B	Σ
O1		0.51 ^{x3} →				1.51
O2	0.17 ^{x3} ↓	0.42 ^{x2} ↓→			0.96	1.98
O3		0.34	0.40 ^{x2} →			1.13
O4	0.07 ^{x3} ↓			0.99 ^{x2} →		2.05
O5	0.10 ^{x3} ↓			0.94 ^{x2} →		1.98
O6		0.45 ^{x2} ↓	0.49	1.04		1.99
O7			0.49	1.07		1.99
			0.43			
O8			0.48		1.00 ^{x2} ↓	2.00
			0.52			
Σ	1.02	2.59	2.81	4.04	2.96	
MFV	1.17	2.62	2.79	4.00	3.00	

*MFV = mean formal valence from site populations.

TABLE 9. Selected properties of oxy-dravite, vanadio-oxy-dravite and oxy-vanadium-dravite.

	Oxy-dravite	Vanadio-oxy-dravite	Oxy-vanadium-dravite
<i>a</i> (Å)	15.9273(2)	16.0273(3)	16.1908(4)
<i>c</i> (Å)	7.2001(1)	7.2833(1)	7.4143(2)
<i>V</i> (Å ³)	1581.81(4)	1620.24(5)	1683.21(7)
Space group	<i>R3m</i>	<i>R3m</i>	<i>R3m</i>
Optic sign	Uniaxial (–)	Uniaxial (–)	Uniaxial (–)
ω	1.650(5)	1.693(5)	1.786(5)
ϵ	1.620(5)	1.673(5)	1.729(4)
Colour	Dark red	Green	Black
Pleochroism	O = orange E = pink	O = yellow green E = pale olive green	O = deep brownish green E = yellow green
Reference	(1)	(2)	(3) and (4)

*(1) Bosi and Skogby (2013); (2) this study; (3) Reznitskii et al. (2001); (4) Bosi et al. (2013a).

FIGURE 1

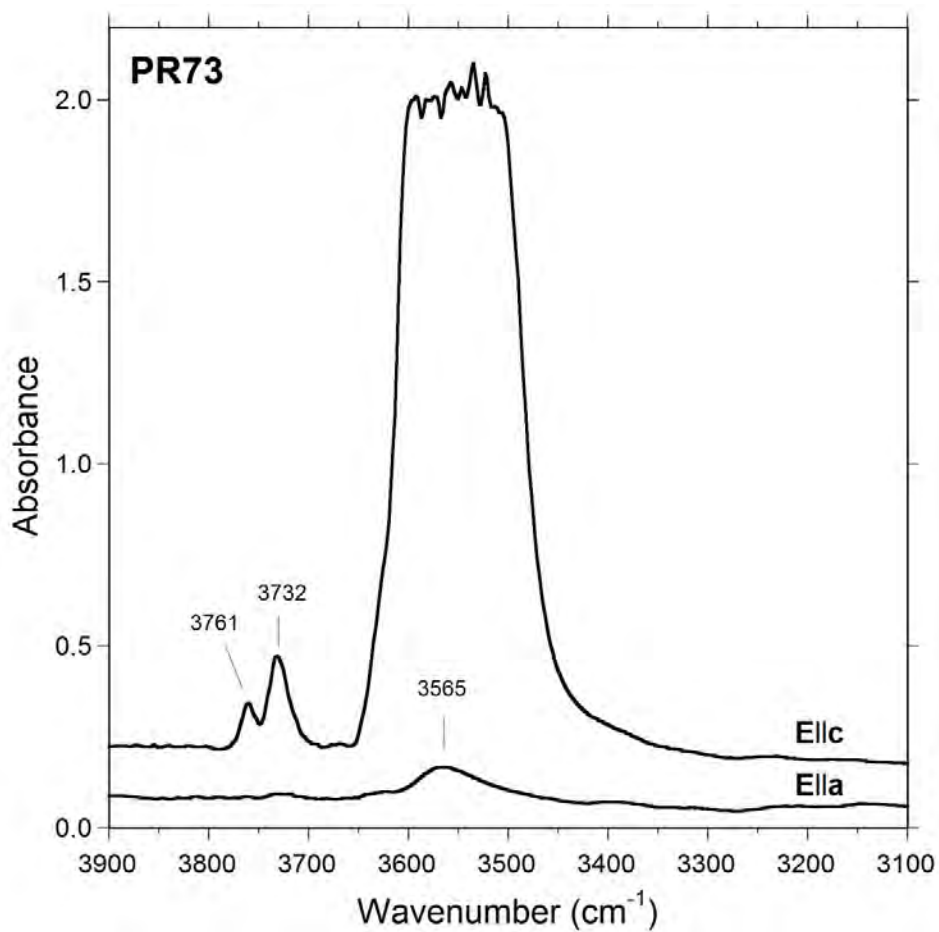


FIGURE 2

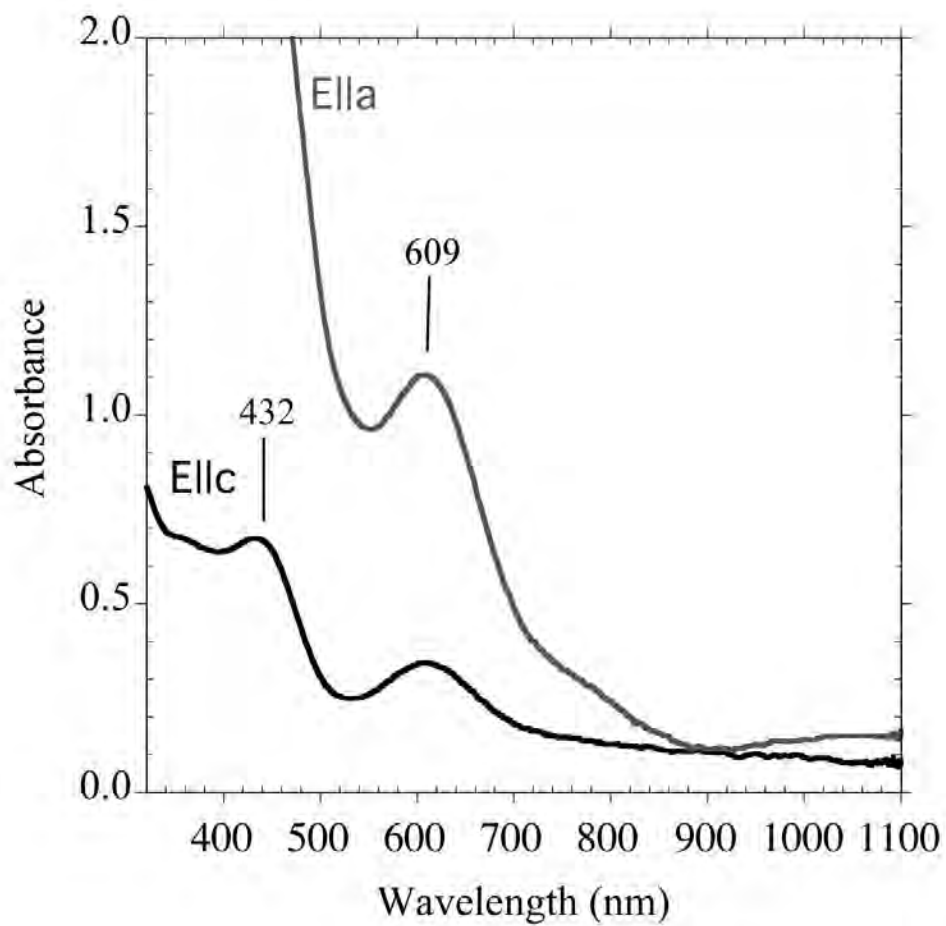


FIGURE 3

